

Fault Displacement Hazard for Strike-Slip Faults

by Mark D. Petersen, Timothy E. Dawson, Rui Chen, Tianqing Cao,
Christopher J. Wills, David P. Schwartz, and Arthur D. Frankel

Abstract In this paper we present a methodology, data, and regression equations for calculating the fault rupture hazard at sites near steeply dipping, strike-slip faults. We collected and digitized on-fault and off-fault displacement data for 9 global strike-slip earthquakes ranging from moment magnitude M 6.5 to M 7.6 and supplemented these with displacements from 13 global earthquakes compiled by [Wesnousky \(2008\)](#), who considers events up to M 7.9. Displacements on the primary fault fall off at the rupture ends and are often measured in meters, while displacements on secondary (off-fault) or distributed faults may measure a few centimeters up to more than a meter and decay with distance from the rupture. Probability of earthquake rupture is less than 15% for cells $200\text{ m} \times 200\text{ m}$ and is less than 2% for $25\text{ m} \times 25\text{ m}$ cells at distances greater than 200 m from the primary-fault rupture. Therefore, the hazard for off-fault ruptures is much lower than the hazard near the fault. Our data indicate that rupture displacements up to 35 cm can be triggered on adjacent faults at distances out to 10 km or more from the primary-fault rupture. An example calculation shows that, for an active fault which has repeated large earthquakes every few hundred years, fault rupture hazard analysis should be an important consideration in the design of structures or lifelines that are located near the principal fault, within about 150 m of well-mapped active faults with a simple trace and within 300 m of faults with poorly defined or complex traces.

Online Material: Description and tables of displacement data, distributed ruptures, mapping accuracy, and regression statistics.

Introduction

Coseismic surface displacements associated with large earthquakes have caused significant damage to structures and lifelines located on or near faults and will impact future structures unless proper structural design or avoidance legislation mitigates this hazard. There are many examples of fault ruptures causing failure or near-failure of bridges (Japan, 1995; Taiwan, 1999; Turkey, 1999), dams (Taiwan, 1999), buildings (California, 1971; Turkey, 1999), railroads (Guatemala, 1976), tunnels (Taiwan, 1999), and pipelines (California, 1971; Alaska, 2001). In spite of these structural failures, this hazard is not considered in current U.S. building code regulations. A few state and local jurisdictions have implemented regulations to avoid this hazard by restricting construction on or near active faults. For example, the California state legislature enacted the 1972 Alquist-Priolo Earthquake Fault Zoning Act (A-P zones), limiting new construction used for human occupancy within 30 m of the mapped trace of an active fault unless comprehensive site-specific geological investigations show that the fault does not pose a significant hazard (see [Data and Resources](#)). Similar legislation has also been implemented in the state of Utah (Salt Lake County) and in New Zealand and Taiwan.

While these laws limit development along and near an active fault trace, they do not provide guidance for mitigating structural damage for nonhabitable structures and lifelines that require fault crossings and may be subjected to ground deformations in large earthquakes.

Engineering solutions have been developed for mitigating the impact of fault rupture on a structure. For example, surface rupture from the 2002 moment magnitude M 7.9 Denali, Alaska, earthquake showed that a major oil pipeline could accommodate several meters of fault displacement when the design allows for considerable flexibility ([Sorensen and Meyer, 2003](#)). These designs could be improved with an estimate of the rate of exceedance of various levels of displacements occurring beneath the structure, or a displacement hazard curve. Consideration of this hazard curve in engineering design is essential in quantifying the financial risks of damage and business disruptions, societal impacts on traffic or loss of utilities from lifeline interruptions, environmental impacts from spills or fires, and health problems resulting from air/water contamination or injuries caused by structural collapse.

Fault displacement data have previously been collected and analyzed by several investigators for assessment of fault rupture characteristics. Fault mechanic studies summarized by Ben-Zion and Sammis (2003) give evidence of a complicated maturation process that involves deformation in a network of disordered faults and ultimate evolution into a system of coalescing faults where the shear is localized into a principal-fault system. They suggest that observed power-law statistics of earthquakes can be generated by physics-based models that involve a complex pattern of shear strain that is distributed over a broad array of fault sizes. Our interest in this paper is to probabilistically characterize the levels of displacements that can occur across this complex-strain field.

Several studies have documented displacements along active strike-slip faults, and these are summarized in Petersen and Wesnousky (1994). Wells and Coppersmith (1994) formulated equations to characterize such displacements on the principal fault. Hemphill-Haley and Weldon (1999) examined fault displacement distributions on the principal fault, determined that rupture displacements often taper off at the end of the ruptures, and showed that displacement variability is independent of magnitude. Biasi and Weldon (2006) inverted these displacement data to obtain magnitude and rupture length probability density functions (PDF) using point measurements of slip data from paleoseismic investigations at sites along the fault. Wesnousky (2008) used fault rupture observations to assess the end points of ruptures and showed that asymmetric slip distributions fit the observations better than more symmetrical models. This observation brings to light the challenges in identifying the end points of future fault ruptures. In addition, Wesnousky (2008) provided evidence for the size distribution of geometrical discontinuities that can restrain rupture propagation. Fault displacements have also been modeled using interferometric synthetic aperture radar (InSAR) and Global Positioning System (GPS) data. While these data may be useful in the future for supplementing the geologic displacement observations, we have not compiled these data for use in this analysis. Research on space geodetic observations indicate that the strain data are compatible with the geologic offsets collected after the 1999 *M* 7.1 Hector Mine earthquake, showing a similar maximum offset with gradual tapering toward the rupture ends (e.g., Fialko *et al.*, 2001).

The fault rupture hazard analysis methodology we develop is an extension of the probabilistic fault displacement hazard assessments developed for the proposed Yucca Mountain high-level nuclear waste repository in Nevada (Stapp *et al.*, 2001; Youngs *et al.*, 2003) and for the Wasatch fault in central Utah (Braun, 2000). The Youngs *et al.* (2003) model describes probabilistic-earthquake- and displacement-based analyses; our study is similar to their probabilistic-earthquake approach. However, these published studies analyzed normal-fault displacements, while our analysis is focused on strike-slip fault displacements observed along the strike and off of the principal fault. In addition, we propose a more complicated model than the previous authors by including the depen-

dency of fault displacement hazard on the accuracy of fault mapping and the complexity of the map trace.

In this paper we present a methodology, data, and regression equations to estimate coseismic strike-slip fault rupture hazard in a deterministic or probabilistic framework. We consider the net fault displacements that include both vertical and horizontal movements (see the electronic supplement to this paper). The analysis does not account for nontectonic displacements. We did not include fault creep, afterslip, displacement due to liquefaction, or landslides. However, some afterslip is most likely incorporated in the fault displacement measurements that were collected several hours to days after the earthquake. The regression equations include six different principal-fault displacement models, two distributed-fault displacement models, and a probability model for rupture displacement. In addition, we show examples of fault rupture hazard assessments for transects and grids across a strike-slip fault with varying mapping accuracy and complexity characteristics. We recommend performing displacement hazard analysis using site-specific data when such data are available. This additional information could result in smaller uncertainties; however, when data are not available for a particular fault, the data and regressions presented here will allow us to estimate the displacement hazard from global data and the associated uncertainties.

Methodology for Calculating Fault-Rupture Hazard

Several parameters are important in determining the coseismic fault-displacement hazard at a site, the size of the earthquake and probability that it will rupture to the surface, the rate of all potential earthquakes on the fault, the potential and amount of displacement along or near the fault, the distance from the site to all potential ruptures, the complexity of the fault and accuracy of the fault mapping, and the size or footprint of the structure that will be placed at the site. To develop the fault rupture hazard methodology, we consider a fault and site (x, y) with the geometry shown in Figure 1. The area we consider for calculating the probability of fault rupture has dimension z (area z^2) and is located a distance r from the fault trace with a distance ratio, l/L , where l is the distance measured from the nearest point on the fault rupture to the closest end of the rupture, and L is total rupture length. The earthquake rupture may not extend along the entire fault but may only extend along a section of the fault located a distance s from the end of the fault. The displacement on the fault is denoted as D , and the displacement at a site off the fault as d . The principal-fault displacements are considered primary ruptures on the main, continuous fault that are located within several meters of the mapped fault. The distributed-fault displacements are off the principal fault and are typically discontinuous ruptures or shears located tens of meters to a few kilometers from the principal fault trace. The principal and distributed-fault displacements represent the net displacements, which include both vertical and horizontal offsets (see the electronic supplement to this paper).

because this has been used in the [Youngs *et al.* \(2003\)](#) fault-displacement hazard model as well as in ground-motion prediction equations (references in [Petersen *et al.*, 2008](#)).

Next, we allow for the variability in rupture location. We define a PDF, $f_R(r)$, to denote the range of perpendicular distances, r , from the site to various potential ruptures. [Youngs *et al.* \(2003\)](#) defines r to be the closest distance to the rupture, which eliminates the need for the variable s (the distance of the rupture along the fault) in the equation. However, we have separated the variable s from r so that r only accounts for location uncertainty perpendicular to the site. A fault typically is a complex shear zone that is made up of coalescing faults and shears. The locations of ruptures may not occur on the exact same trace during subsequent earthquakes; we think that faults must evolve through time, creating new fault traces. This aleatory variability would account for the random location of future earthquakes, a quantity that is not presently well defined. In addition, there are uncertainties associated with the fault mapping quality and complexity of the fault trace as well as the inaccuracies in mapping the fault that translate into an epistemic uncertainty in the location of future ruptures. Our PDF for r includes both aleatory and epistemic components.

We evaluated the probability of rupture displacement D greater than some level D_0 at site (x, y) that is on or near the fault (generally within a few hundred meters) and over an area of z^2 . Similarly, we also evaluated the probability that off-fault displacement d is greater than or equal to d_0 at a location (x, y) off the fault and within an area z^2 . This area could represent the building foundation size or the footprint of the building. The displacement on and off the principal fault, D and d , respectively, can also be characterized as including components of epistemic uncertainty and aleatory variability. The epistemic uncertainty is related to measurement errors of displacements along the fault rupture. The aleatory variability is related to the natural variability in the along-fault displacements between earthquakes.

We define the annual rate of exceedance as

$$\begin{aligned} \lambda(D \geq D_0)_{xyz} &= \alpha(m) \int_{m,s} f_{M,S}(m, s) P[sr \neq 0 | m] \\ &\quad \times \int_r P[D \neq 0 | z, sr \neq 0] \\ &\quad \times P[D \geq D_0 | l/L, m, D \neq 0] f_R(r) dr dm ds \end{aligned} \quad (1)$$

for principal-fault contributions, and

$$\begin{aligned} \lambda(d \geq d_0)_{xyz} &= \alpha(m) \int_{m,s} f_{M,S}(m, s) P[sr \neq 0 | m] \\ &\quad \times \int_r P[d \neq 0 | r, z, sr \neq 0] \\ &\quad \times P[d \geq d_0 | r, m, d \neq 0] f_R(r) dr dm ds \end{aligned} \quad (2)$$

for distributed-fault contributions.

In some established methodologies, such as that developed by [Youngs *et al.* \(2003\)](#), the hazard is related to the average or maximum principal-fault displacements for a given magnitude. In this paper we develop regression equations and PDFs for (1) displacements as a function of magnitude and distance as well as (2) for normalized displacements along the main fault that are a function of the average displacement on the fault, D_{ave} . The equations relating the displacements on and off the fault to the average displacements (normalized displacements) can be written, respectively, as

$$\begin{aligned} P[D \geq D_0 | l/L, m, D \neq 0] \\ = \int_{D_{ave}} P[D \geq D_0 | l, L, D_{ave}(m), D \neq 0] \\ \times f_{D_{ave}}[D_{ave}(m)] dD_{ave}, \end{aligned} \quad (3)$$

and

$$\begin{aligned} P[d \geq d_0 | r, m, d \neq 0] \\ = \int_{D_{ave}} P[d \geq d_0 | r, D_{ave}(m), d \neq 0] f_{D_{ave}}[D_{ave}(m)] dD_{ave}. \end{aligned} \quad (4)$$

When normalized displacement regressions are used, equations (3) and (4) should be inserted into equations (1) and (2) to calculate the exceedance probability term. These formulas are used to assess the probabilistic normalized-fault displacement hazard at a site. If one desires to calculate the deterministic fault displacement hazard, the formula can be modified by eliminating the rate parameter, α , from the equation. Alternatively, one can calculate the median displacements for a particular earthquake using the empirical data and relations that are described in the following sections. The mean and eighty-fourth percentile displacements can be calculated using the median and uncertainties associated with each equation.

Data

To assess fault-rupture hazard, we rely on three input data sets: (1) similar-scale maps of surface rupture produced following an earthquake, which depict the rupture trace; (2) large-scale fault maps produced prior to an earthquake rupture, which depict what is referred to here as the mapped trace; and (3) displacement data compiled along faults that ruptured during an earthquake, including displacements along the fault that ruptures coseismically. The fault maps produced prior to an earthquake can be compared to the location of surface ruptures produced by an earthquake along that fault in order to quantify how well the geological maps predicted the location of surface rupture along the fault. For this analysis, displacement observations are needed for locations along the strike of the fault, as well as for locations away from the principal-fault trace. These data can be regressed, and those equations can then be applied to other mapped faults to probabilistically assess the location of surface ruptures in future earthquakes.

We collected and digitized displacement data from published rupture displacement measurements of the following large strike-slip earthquakes: 1968 Borrego Mountain (M 6.5), 1979 Imperial Valley (M 6.5), 1987 Superstition Hills (M 6.5), 1992 Landers (M 7.3), 1995 Kobe (M 6.9), 1999 Izmit, Turkey (M 7.6), 1999 Duzce (M 7.1), and the 1999 Hector Mine (M 7.1) earthquakes (Table 1 and $\text{\textcircled{E}}$ electronic supplement to this paper). These earthquake ruptures were selected for our analysis because large-scale, detailed rupture maps are available as well as a dense sampling of displacement measurements both along the rupture as well as along other faults that ruptured during the earthquake. A number of other historical strike-slip earthquake ruptures were not included in this analysis due to a lack of detailed slip measurements or a lack of detailed mapping along the length of the rupture. We supplemented these data with the principal-fault strike-slip displacement data compiled by Wesnousky (2008) that extends the displacement data to earthquakes up to M 7.9. Figure 2 shows the magnitudes and distances that are included in our displacement data. The data for on-fault displacements cover a broad range from M 6.3 to M 7.9 (Fig. 2a). Data for distributed-fault displacements are sparser but also cover an important range of magnitudes between M 6.5 and M 7.6 (Fig. 2b). The off-fault displacement data developed for this analysis are primarily based on perpendicular distances from the mapped fault trace to the nearest rupture but also include a few secondary ruptures off the ends of the faults. Figure 2c shows the off-fault displacement data and indicates that 35-cm displacements can be triggered on faults more than 10 km away from the principal fault. Measured fault displacements include measurement errors as well as observation limitations and constraints.

To assess the location (epistemic) uncertainty between the mapped trace and the rupture trace, we compiled large-scale (1:24,000) fault maps that were produced prior to the historical surface-rupturing earthquakes and compared them to maps produced following the earthquake. For this analysis, we digitized A-P zones and other published material ($\text{\textcircled{E}}$ see the electronic supplement to this paper) to compare with the observed fault rupture traces. In California, legislation requires the State Geologist to identify those faults that are “sufficiently active and well-defined” to represent a sur-

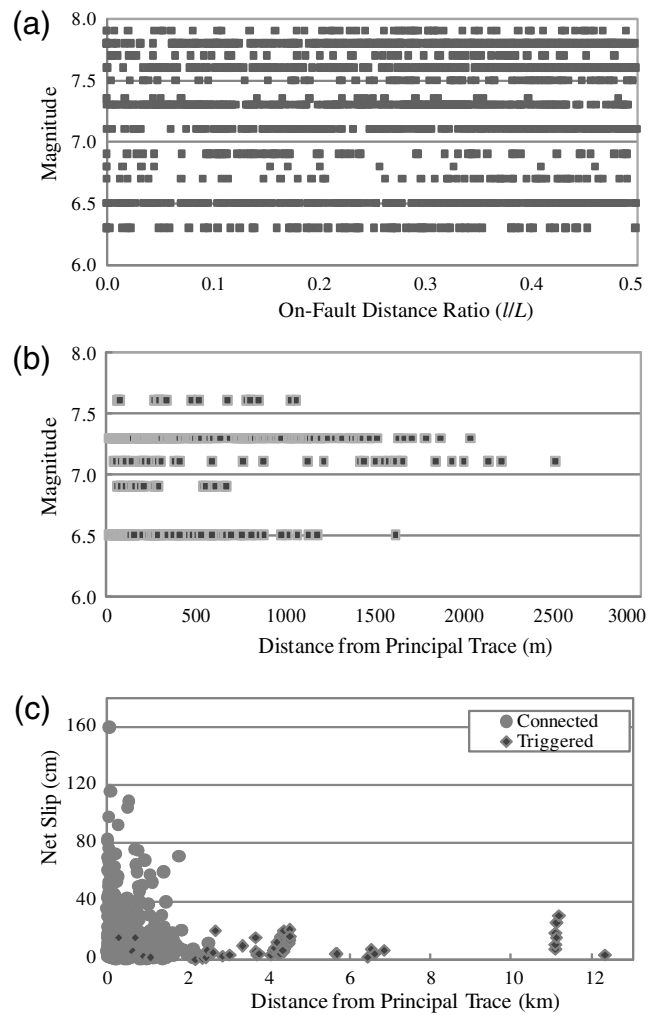


Figure 2. Distribution of displacement data: (a) Principal-fault displacement data used in regressions for magnitude and position along the fault (l/L). (b) Distributed off-fault displacement data used in regressions for magnitude and distance from the mapped fault. (c) Distributed-fault displacement data (labeled as connected) showing net slip as a function of distance from the mapped fault. Triggered rupture displacements are plotted but are not used in the regressions.

face-rupture hazard. To accomplish this, the California Geological Survey (CGS) examines the majority of the potentially active faults in the state and prepares detailed

Table 1
Maximum and Average Displacements Used in This Study

Earthquake	Moment Magnitude*	Maximum Displacement (cm)	Reference	Average Displacement (cm)	Reference
1968 Borrego Mt.	6.5	38	Clark (1972)	18	Wells and Coppersmith (1994)
1979 Imperial Valley	6.5	78	Sharp <i>et al.</i> (1982)	43	Sharp <i>et al.</i> (1982)
1987 Superstition Hills	6.5	90	Sharp <i>et al.</i> (1989)	43	Wells and Coppersmith (1994)
1992 Landers	7.3	670	CGS, unpublished	295	Wells and Coppersmith (1994)
1995 Kobe	6.9	210	Awata and Mizuno (1998)	140	Awata and Mizuno (1998)
1999 Izmit	7.6	510	Langridge <i>et al.</i> (2002)	210	This study
1999 Hector Mine	7.1	525	Treiman <i>et al.</i> (2002)	250	Treiman <i>et al.</i> (2002)
1999 Duzce	7.1	500	Akyuz <i>et al.</i> (2002)	300	Akyuz <i>et al.</i> (2002)

*USGS preferred magnitudes (http://earthquake.usgs.gov/aboutus/docs/020204mag_policy.php).

maps of those that can be shown to have ruptured to the ground surface in Holocene time. These faults are included in A-P zones, which regulate development near active fault traces. A-P maps are particularly suitable for this analysis because the maps are compiled on a large scale, and the mapped fault traces are symbolized by their relative location uncertainty. Faults mapped for A-P zones show the surface traces of the faults in four categories based on how clearly and precisely they can be located. Those four categories: accurately located, approximately located, inferred, and concealed are shown on the A-P maps with different line symbols.

In general, the accuracy of the fault location is a function of the geomorphic and geologic conditions that affect the ability of the geologist to recognize and interpret the fault, as well as the ability to accurately transfer that spatial information onto a base map or digitally in the geographic information system (GIS). For example, a fault map is typically produced by a geologist using imagery such as aerial photography, interpreting the faulting patterns from geomorphology, and transferring the fault locations to a base map or GIS platform having some geographical projection that allows others to locate the fault on the earth's surface. In many cases the fault may be difficult to identify because sediment deposition and erosion may obscure or conceal the surface fault, leading the geologist to classify the fault trace as concealed, or inferred, both of which likely have considerable uncertainties in the actual location of the fault. Additional epistemic location uncertainty is introduced due to limitations in the accuracy of the base map or imagery or to the precision of the equipment used to transfer this information to a map or database. For example, while an easily recognized feature such as a fault scarp is classified as well located, the accuracy of its location is still limited by the accuracy of the base map that it is plotted on. On a typical U.S. Geological Survey (USGS) 1:24,000-scale topographic map, the USGS states that "the horizontal accuracy standard requires that the positions of 90% of all points tested must be accurate within 1/50th of an inch" (USGS, 1999). At 1:24,000 scale, one fiftieth of an inch is 40 ft, or about 12 m. Gauging the cumulative effects of all of these sources of location uncertainties is a key element in assessing fault-rupture hazard for a site, especially in cases where the best available fault maps are of similar scale to the ones used in this analysis. Site investigations that include detailed mapping and trenching studies are a preferred step in reducing the uncertainties in displacements at a particular site.

Figure 3a illustrates how we assessed mapping accuracy for this study. Once the mapped traces of the fault and the rupture traces were digitized into a GIS database (described in the  electronic supplement to this paper), we sampled at intervals along the mapped trace, measuring the distance to the rupture trace. Our measurements are derived from two methods: (1) samples taken evenly every 0.5 km along the fault and (2) samples taken at the midpoints and end points of all ruptures. The second sampling method was considered

because we noticed that many short mapped fault traces were being missed by sampling at fixed intervals along the fault. However, with the exception of the concealed uncertainty category, the values of principal-fault displacements are quite insensitive to the sampling technique. Thus, for our analysis, we have used data derived from both types of sampling. Table 2 summarizes the average and standard deviations for displacements observed in these strike-slip earthquakes for the different mapping accuracy categories. Note that distances are all positive because the data do not distinguish between different sides of the fault. The mean is not centered over the fault with zero distance. Therefore, we apply a statistical function to convert the one-sided sigma to the two-sided sigma that is centered over the fault (Tables 2–3):

$$\sigma = \sqrt{\sigma'^2 + \mu^2},$$

where σ' is the one-sided sigma in Tables 2 and 3 and μ is the mean distance from the principal fault to the surface rupture (in meters).

An additional element we have tried to capture in our analysis is the effect of fault complexity on mapping accuracy. Fault complexity is typically observed at locations where the fault changes strike, where the fault splays, where the fault steps over to a new trace, and where the fault terminates. Figure 3b illustrates this variability by comparing two areas along the 1999 Hector Mine earthquake rupture. Figure 3c shows a relatively simple fault trace consisting of a narrow zone of *en echelon* surface breaks. In contrast, Figure 3d, plotted at the same scale, illustrates a complex zone of faults within a 100- to 200-m right step in the fault zone. In these complicated sections, earthquake ruptures often extend over a broader region, making it more difficult for the geologist to recognize discrete fault traces, which in turn, influences the fault-rupture hazard. For this fault-rupture analysis, we characterize the complexity of the fault at each sampled mapped trace location as either simple (a relatively straight part of the fault zone) or complex (within a geometric feature such as a stepover, bend, or end of a mapped fault). We also calculate the uncertainties associated with simple or complex classifications for inferred or concealed faults (Table 3). We limit our fault complexity analysis to the inferred and concealed categories. The mapped traces are typically classified as inferred or concealed where there are geometric changes in the fault, likely due to the fault being poorly expressed within these areas prior to the rupture. Very few of the accurately and approximately located measurements were classified as complex. Therefore, we did not subdivide the complexity beyond the concealed and inferred categories. Typically, the rupture displacements are related to the map characteristics, with the smallest errors associated with accurate simple traces and the greater errors with complex inferred or concealed faults traces (Tables 2 and 3). This mapping accuracy is an epistemic uncertainty and can be reduced with additional information. Normally

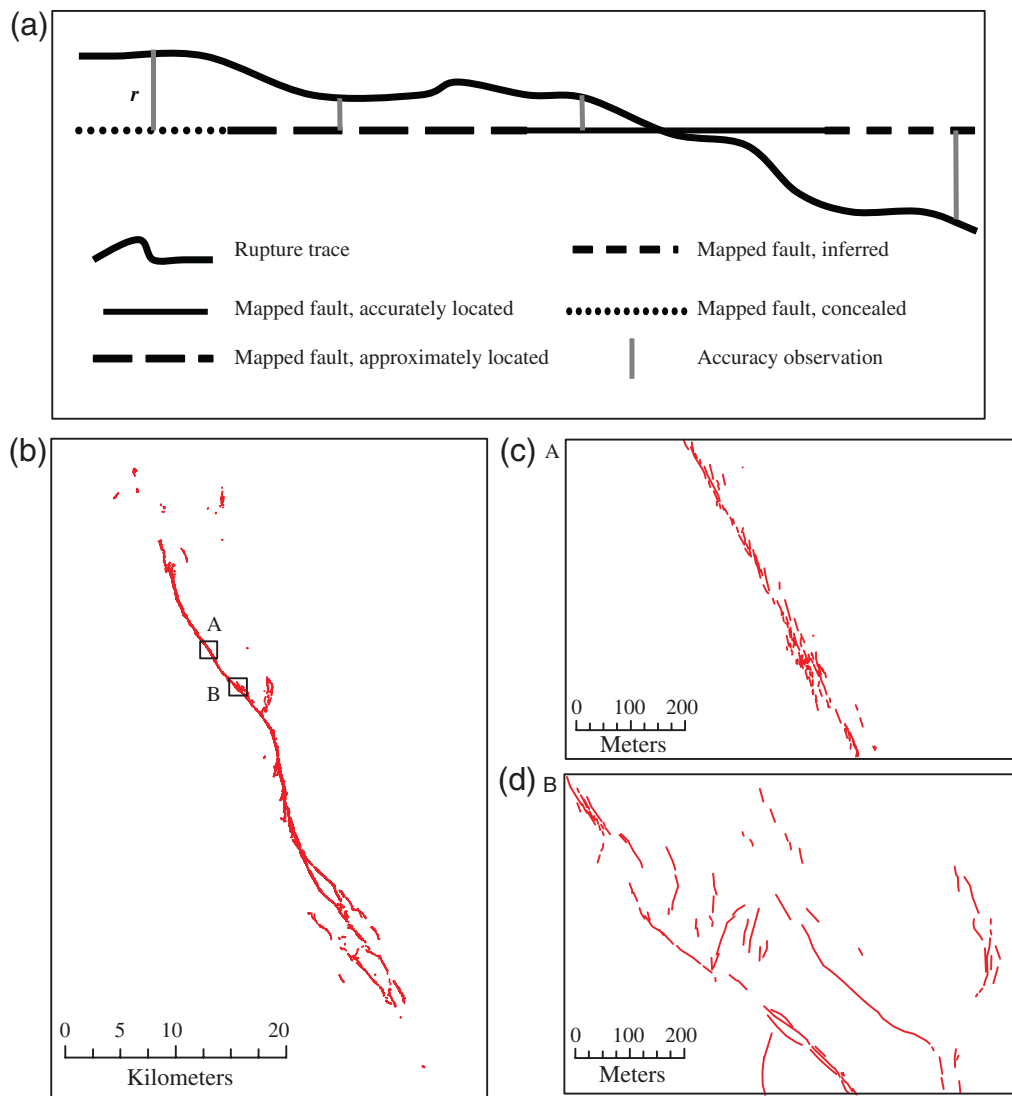


Figure 3. Illustration of mapping uncertainty and fault complexity: (a) Schematic diagram showing how the distance between the rupture trace and the mapped fault was measured, where r is the distance between the preearthquake mapped fault trace and the location of the earthquake surface rupture. (b) Rupture map from the Hector Mine earthquake, modified from Treiman *et al.* (2002); the two boxes labeled A and B are shown in more detail in parts (c) and (d). (c) Area of box A shown in (b), illustrating a relatively simple, narrow zone of surface ruptures along the Hector Mine earthquake rupture. (d) Area of box B, showing a complex, distributed zone of surface ruptures, where the fault takes a ~100-m right step. Note that (c) and (d) are plotted at the same scale.

this epistemic uncertainty should be considered as alternative branches in a logic tree. However, we do not have geologic data to separate the aleatory variability from the epistemic uncertainty.

In general, the data and regressions show what a geologist would expect, that the accurately located and approximately located traces more accurately predict the surface-rupture location. Inferred and concealed traces have greater variability in distance from the surface ruptures, although these distinctions are not as clear as one might expect. Generally, many of the primary ruptures have been located within 100 m of simple well-mapped faults. In contrast, many of the primary ruptures from complex inferred and concealed traces have been located at twice or three times those distances. Although we have not systematically looked over the data to examine the reasons

why the rupture trace deviated from the mapped trace, in general, the preevent mapping is often not aligned directly with the earthquake surface rupture for any of the following reasons: (1) the previous fault mapping was not accurate enough

Table 2
Mapping Accuracy Summary: Distance Measured from Mapped Fault Trace to Observed Surface Rupture

Mapping Accuracy	Mean (m)	One-Sided Standard Deviation (m)	Two-Sided Standard Deviation On Fault (m)
All	30.64	43.14	52.92
Accurate	18.47	19.54	26.89
Approximate	25.15	35.89	43.82
Concealed	39.35	52.39	65.52
Inferred	45.12	56.99	72.69

Table 3
Complexity Summary: Distance Measured from Mapped Fault Trace to Observed Surface Rupture

Complexity	Mean (m)	One-Sided Standard Deviation (m)	Two-Sided Standard Deviation On Fault (m)
Simple, concealed	36.58	49.96	61.92
Simple, inferred	31.49	38.29	49.57
Complex, concealed	90.31	73.12	116.2
Complex, inferred	83.23	81.30	116.35

for the assessment, (2) the fault trace could not be identified or was misinterpreted from the geomorphic features, and (3) the rupture did not occur along the same fault strands that ruptured in previous events.

For assessing off-fault secondary rupture hazard, we followed the methodology of [Youngs et al. \(2003\)](#) and digitized the off-fault rupture and displacement data up to 12 km from the fault rupture. The probability of rupture was assessed by calculating the number of cells that contain ruptures and the total number of cells. In contrast to [Youngs et al. \(2003\)](#), who use a set 500×500 m cell size, we used a variety of square cells that range from 25 to 200 m on a side (Tables 4 and 5) in order to better represent the range of areas upon which structures will be built. Many of the displacements beyond 2-km distances are triggered ruptures on other faults. We have removed these triggered ruptures for this analysis but recognize that adjacent faults are an important source of fault-rupture hazard and should be considered in the analysis separately. These displacement data form the basis of all the PDFs needed for the analysis.

Published Data and Regression Equations for Fault-Rupture Hazard Analysis

In this section, we describe published equations that are needed for a typical fault-rupture hazard assessment. Many of the inputs used to calculate the fault rupture hazard may be obtained from published ground-motion hazard studies. For example, the USGS and CGS have produced seismic ground-shaking hazard models for the U.S. that define potential sizes, locations, and rates of earthquakes on a fault ([Frankel et al., 2002](#); [Petersen et al., 1996; 2008](#)). These fault rupture models may be used to construct the PDFs for magnitude and rupture source, $f_{M,S}(m, s)$, and the earthquake rate parameter α (see [Data and Resources](#)). For site-specific analyses, however, we would recommend obtaining a large-scale

map (at least 1:24,000 scale) to define the location of the fault trace or perform a geologic investigation to analyze the fault location and rupture characteristics. We encourage that site-specific studies be performed on observed historic and paleoseismic displacements on a fault.

Another important input for the assessment is a function that describes the likelihood of a particular-size earthquake reaching the surface. For our analysis, we applied the global empirical formulation developed by [Wells and Coppersmith \(1993\)](#). Their equation for calculating the probability of surface rupture is given by a logistic regression model (commonly applied when the dependent variable is dichotomous) that provides the conditional probability of surface rupture:

$$P[sr \neq 0|m] = \frac{e^{(a+bm)}}{1 + e^{(a+bm)}}, \quad (5)$$

where $sr \neq 0$ implies that the surface rupture is nonzero, m is moment magnitude, and constants a and b are -12.51 and 2.053 , respectively. This equation implies a probability of 87% that an M 7 earthquake will rupture to the surface and 95% that an M 7.5 earthquakes will rupture up to the surface. Other relationships could be based on local/regional data for surface-rupturing events if these data are available.

To calculate the average on-fault displacements, D_{ave} , which is needed for the normalized regressions, we have applied the [Wells and Coppersmith \(1994\)](#) equation for strike-slip faults. They derived the formula

$$\log_{10}(D_{ave}) = a + bm \pm \varepsilon, \quad (6)$$

where D_{ave} is in meters; a is -6.32 ; b is 0.90 ; and ε , the standard deviation in \log_{10} units, is 0.28 . This analysis analyzed displacements from earthquakes with M 5.6 to 8.1. The average displacement data that we used in this study are consistent with the [Wells and Coppersmith \(1994\)](#) data

Table 4
Probability of Distributed-Fault Rupture for Different Cell Sizes

Cell Size (m ²)	$a(z)$	$b(z)$	σ (standard deviation)
25 × 25	-1.1470	2.1046	1.2508
50 × 50	-0.9000	0.9866	1.1470
100 × 100	-1.0114	2.5572	1.0917
150 × 150	-1.0934	3.5526	1.0188
200 × 200	-1.1538	4.2342	1.0177

Table 5
Probability of Distributed-Fault Rupture Interpolation Points

Cell Size (m ²)	p_0 (%)	p_1 (%)	p_2 (%)	r_1 (m)	r_2 (m)
25 × 25	74.541	7.8690	2.0108	100	200
50 × 50	87.162	4.8206	2.6177	100	200
100 × 100	90.173	18.523	6.6354	100	200
150 × 150	87.394	19.592	7.0477	150	300
200 × 200	92.483	18.975	7.4709	200	400

and their strike-slip regression equation (Fig. 4). Other equations besides Wells and Coppersmith (1994) could also be used in an analysis.

Regression Analysis for Strike-Slip Displacements

The rupture displacements we analyzed on the principal fault are very scattered but are generally largest near the middle of the fault and fall off rapidly along the 25–30% of the length towards the end of the rupture. Figure 5 shows our regression models and the data (color-coded by magnitude). In our data set, however, some of the earthquakes have their highest displacements near the end of the rupture (e.g., 1968 Borrego Mountain). Wesnousky (2008) also showed that many of the fault rupture data he compiled also exhibited asymmetrical ruptures. We currently do not have a method to determine which areas of a rupture will exhibit larger displacements. Therefore, asymmetric displacement distributions along the strike of the fault will translate into greater uncertainties, especially near the ends of faults. Displacement data tend to scale with both magnitude and position on the rupture, l/L . We analyzed the dispersion of the on-fault displacement data and regression outputs by comparing the median (D_{50}) and the sixteenth (D_{16}) and eighty-fifth (D_{85}) percentiles. We find that the data are more scattered in the lower half of the distribution than in the upper half (Fig. 5). We also conclude D_{84}/D_{50} is lower and D_{50}/D_{16} is higher than the standard deviation of the regression.

We develop least-squares, best-fit regression equations for the natural log of displacement that consider magnitude, distance, or average displacement for several functional forms. We assume that D/D_{ave} does not depend on M , because the magnitude dependence is considered in the computation of D_{ave} . However, when regression relationships based on normalized displacements are used, one needs to combine aleatory uncertainty from the D/D_{ave} regression

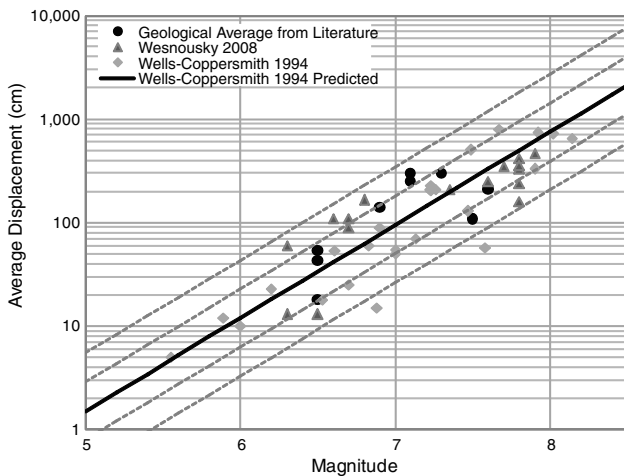


Figure 4. Comparison of the average displacement data from geologic literature and Wesnousky (2008) with those of Wells and Coppersmith (1994). All data fall within the two standard deviations of the Wells and Coppersmith (1994) regression.

as well as aleatory uncertainty from calculating D_{ave} . For both the magnitude-distance and the normalized data, we have applied three models to analyze the principal-fault displacements. Taking the exponential of the resulting values from these regression equations will yield the median displacement. To obtain the mean displacement, we use the following equation:

$$D_{\text{mean}} = e^{\mu + \sigma^2/2}.$$

Residuals for the principal-fault displacement regressions using the bilinear, quadratic, and elliptical models are shown in Figure 6. The residuals for both on-fault distances (l/L) and magnitude (m) are similar for the three models. The residuals for distances cover a wide range and appear to be larger for distances (l/L) less than 0.1 or 0.2. The residuals for distance and magnitude are quite scattered but are centered near zero. Regression statistics may be obtained in the $\text{\textcircled{E}}$ electronic supplement to this paper.

Displacements off the principal fault (distributed faults) decay slightly at distances out to several kilometers (Fig. 7a). Furthermore, displacements also correlate with magnitude. Figure 7a shows that rupture displacements for the large magnitude events cause the largest displacements, while smaller magnitude events cause displacements that are generally lower. However, these correlations are weak, and in earlier versions of this analysis, we did not account for any decay with distance.

Triggered ruptures contribute to this uncertainty because ruptures on adjacent faults may not have the same rupture characteristics as secondary, distributed faults. Ben-Zion and Sammis (2003) indicate that in early stages of fault development, faults deform through a strain-hardening processes, and the fault is characterized with granularity and fractal structures at several levels. The fault evolves with relatively small initial strains into tabular primary slip zones that deform through strain-weakening processes. Finally, smaller faults coalesce into long through-going faults where more regular geometry and deformation takes place through dominant strain-weakening processes. Principal faults in this analysis are more mature faults, while distributed faults may be at earlier stages of development. Triggered faults are assumed to occur on mature strands that are related to principal faulting. Therefore, the physics governing the deformation of triggered ruptures would, most likely, be more similar to that operating on principal faults.

For this paper, we implemented a multivariate regression analysis that considers both magnitude, m , and distance, r , without triggered displacements included in the data set. This should really not affect our results, because we recommend that these equations only be used out to 2 km away from the rupture and not beyond. Most triggered displacements are beyond 2-km distance. We include the triggered data in the $\text{\textcircled{E}}$ electronic supplement to this paper in case a user would like to consider this type of rupture. In the following subsections, we consider magnitude and distance correlations with

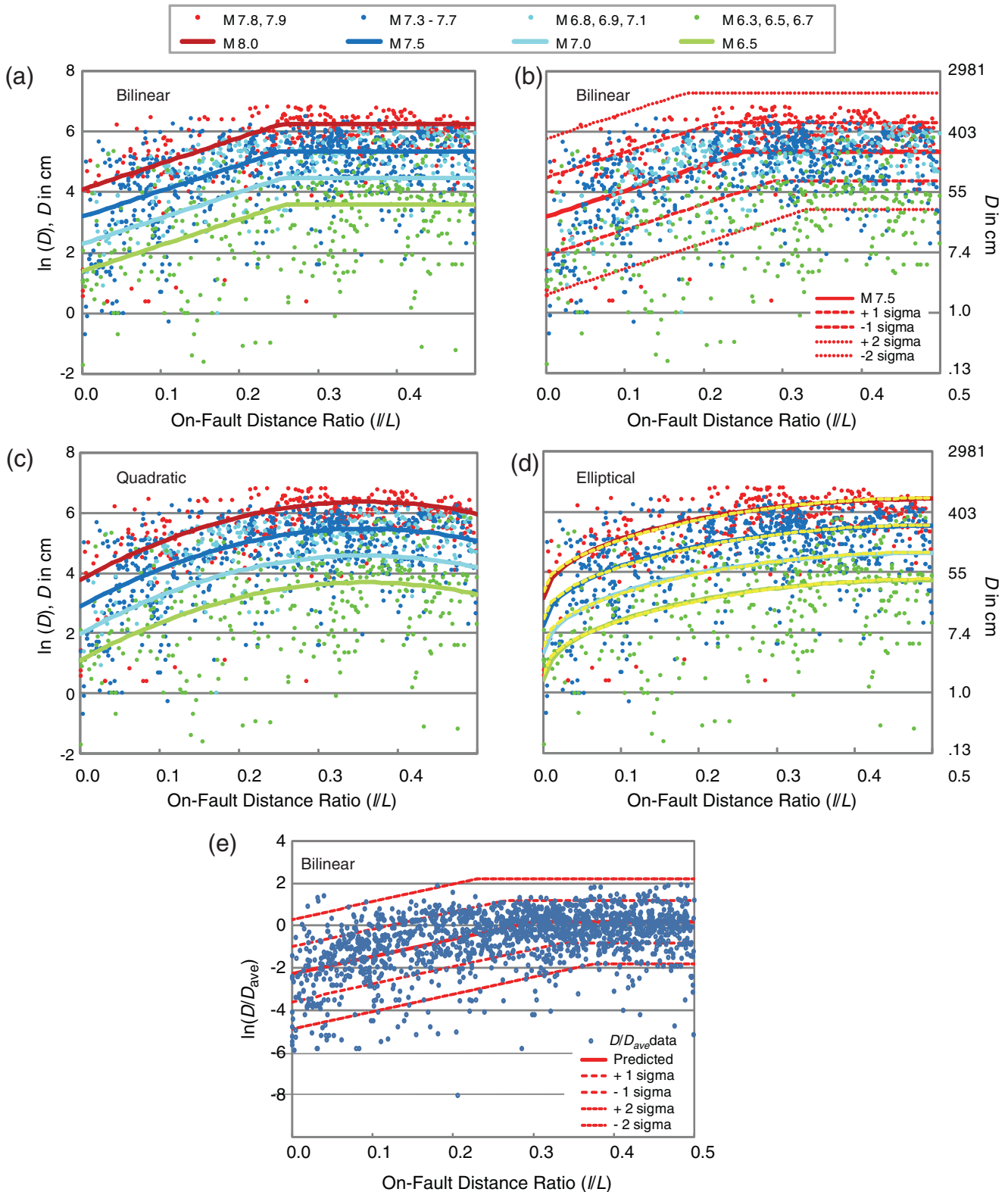


Figure 5. Principal-fault displacement data color-coded by magnitude and regression models (a) with bilinear regression lines for M 6.5 to 8.0, (b) with the bilinear regression lines for M 7.5 and uncertainties of ± 1 and ± 2 standard deviations, (c) with quadratic regression curves for M 6.5–8.0, (d) with the elliptical regression curves for M 6.5 to 8.0 as well as regression curves based on Biasi and Weldon (2009) functional form (dashed yellow curves), and (e) normalized principal-fault displacement data (D/D_{ave}) with bilinear regression line and uncertainties (± 1 and ± 2 standard deviations).

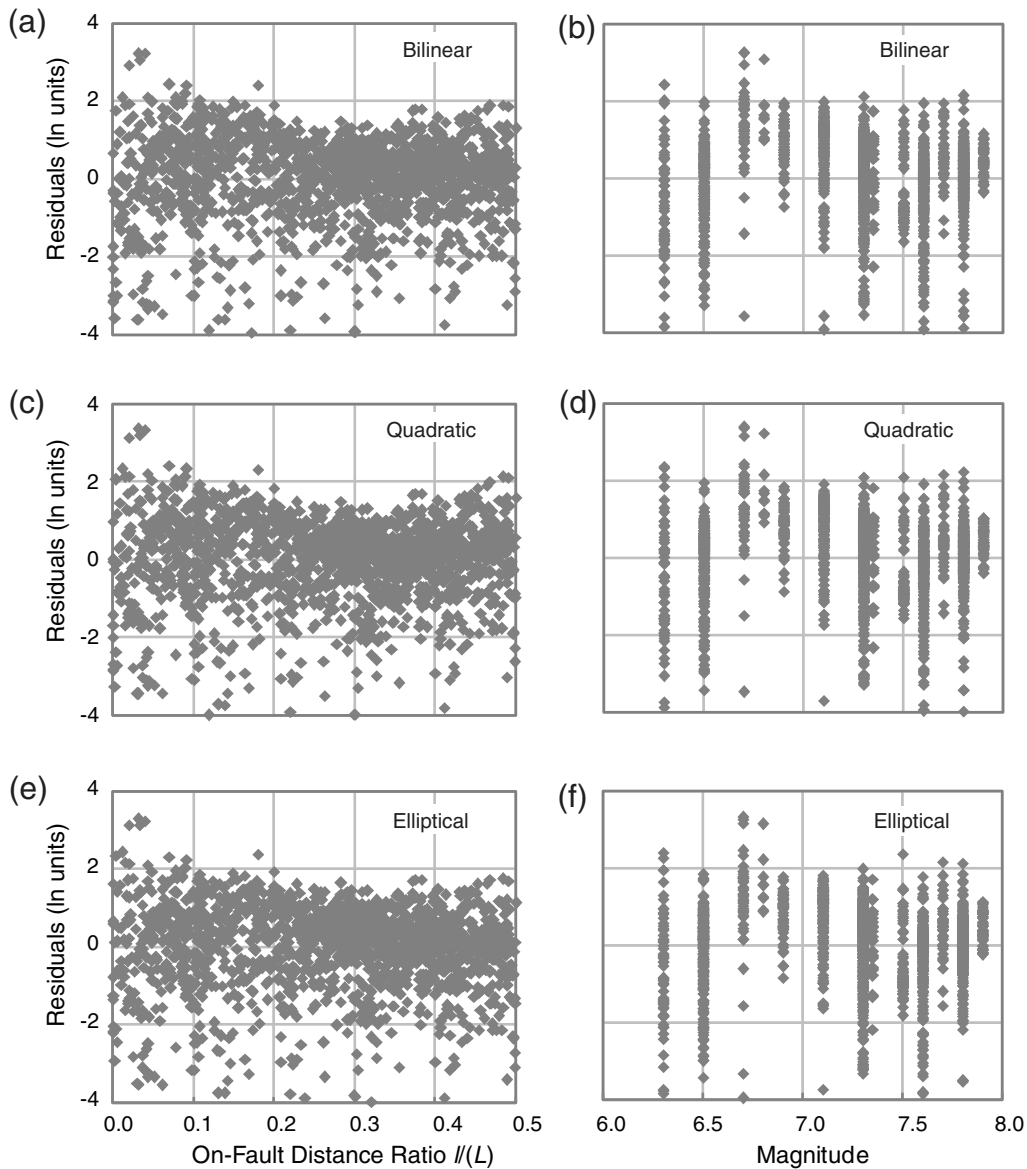


Figure 6. Residuals for principal-fault displacement regressions of the (a) and (b) bilinear model, (c) and (d) quadratic model, and (e) and (f) elliptical model.

distributed-fault ruptures as well as correlations with data normalized by the average principal-fault displacement. We also calculate the probability of having rupture displacements in areas ranging from 25 m × 25 m cells to 200 m × 200 m cells (Fig. 8; Tables 4 and 5).

Regressions were performed on five sets of data: (1) principal-fault displacement data (D , in centimeters), (2) normalized principal-fault displacement data (D/D_{ave}), (3) distributed-fault displacement data (d , in centimeters), (4) normalized distributed-fault displacement data (d/D_{ave}), and (5) off-fault rupture probability data. We develop three models for this analysis: (1) a bilinear model that allows for constant displacements near the middle of the rupture and a linear taper at the ends of the rupture, consistent with principal-fault displacements observed in our data set; (2) a poly-

nomial model that predicts slightly lower displacements at the middle of the fault, consistent with asymmetric rupture models where the displacements may be higher near the ends of the faults as described in Wesnousky (2008); and (3) an elliptical model that curves at the end and is preferred by Biasi and Weldon (2006). The three principal-fault models account for different aleatory uncertainties along the fault and different decay rates at the end of the rupture. We discuss details of the regressions in the following subsections.

Analysis of Principal-Fault Displacements: Function of Magnitude and Distance

Figure 5a is a scatter chart showing the distribution of the raw displacement data and the regression model for the bilinear case. The data reveal a flat portion in the middle of

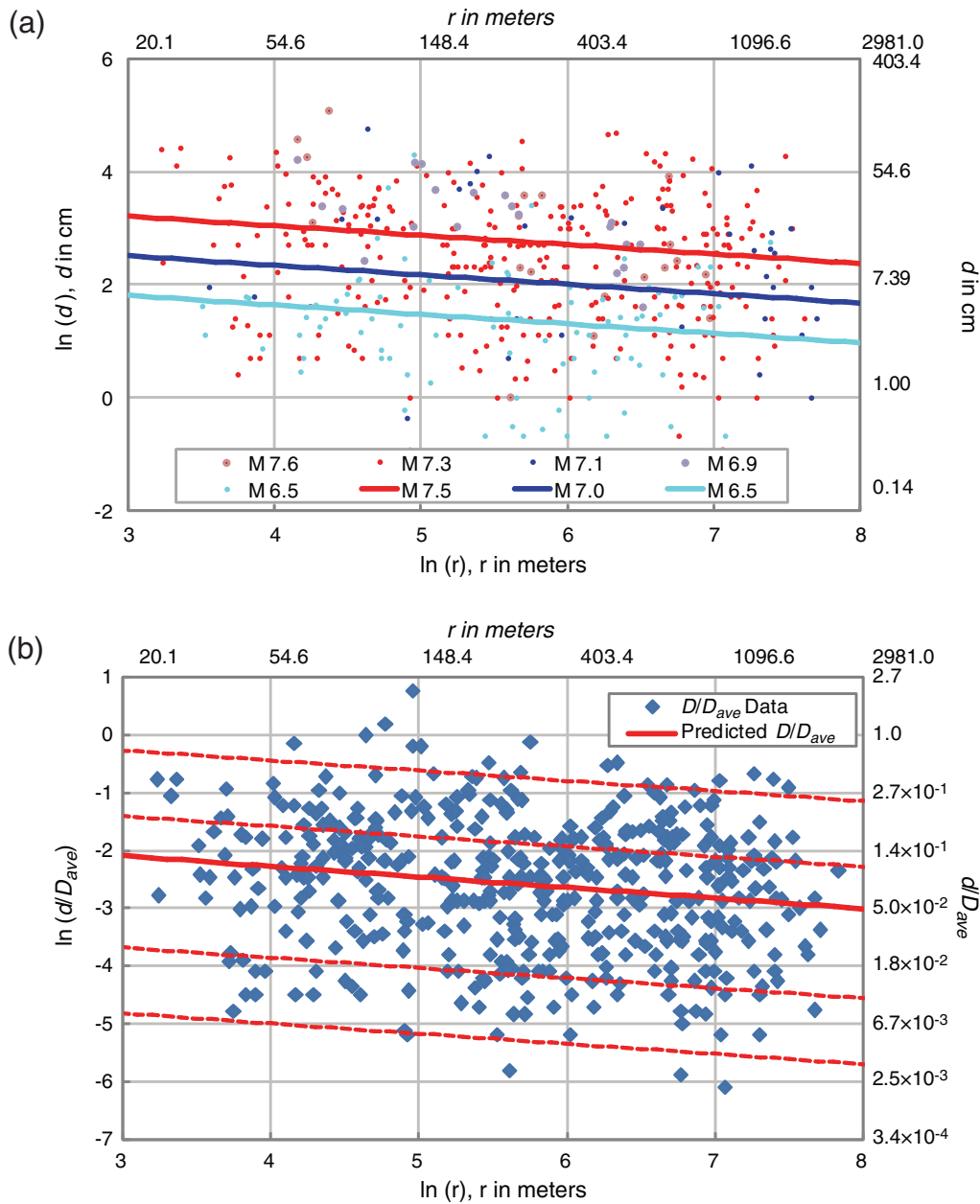


Figure 7. Distributed-fault displacement data and (a) regression displacements color-coded by magnitude with bilinear regression lines for M 6.5 to 7.5, and (b) normalized displacements with bilinear regression line and uncertainties (± 1 and ± 2 standard deviations).

the fault (l/L greater than approximately 0.3). The displacements tend to decrease toward the ends of the fault (as l/L decreases). Therefore, our first statistical model is bilinear. The data are divided into two groups. The first group is for $l/L < 0.3$ (arbitrarily chosen based on the scatter chart). We assume that displacement changes linearly with respect to l/L and m and can be modeled by the following regression equation:

$$\ln(D) = a_1 m + b(l/L) + c_1, \quad (7)$$

where a_1 , b , and c_1 are regression coefficients. The regression coefficients are $a_1 = 1.7969$, $b = 8.5206$, and $c_1 = -10.2855$. The standard deviation is 1.2906 in \ln (natural

\log) units. The second group of data is for $l/L \geq 0.3$. Figure 5a shows that the on-fault displacement does not display apparent dependence on l/L when $l/L \geq 0.3$. Therefore, we eliminate the l/L term in equation (7) and use the following equation to model this portion of the data:

$$\ln(D) = a_2 m + c_2. \quad (8)$$

The regression analysis yields $a_2 = 1.7658$ and $c_2 = -7.8962$, with a standard deviation on $\ln(D)$ of 0.9624. The l/L value where the two linear portions intersect, $(l/L)'$, can be determined by setting equations (7) and (8) equal and solving for l/L :

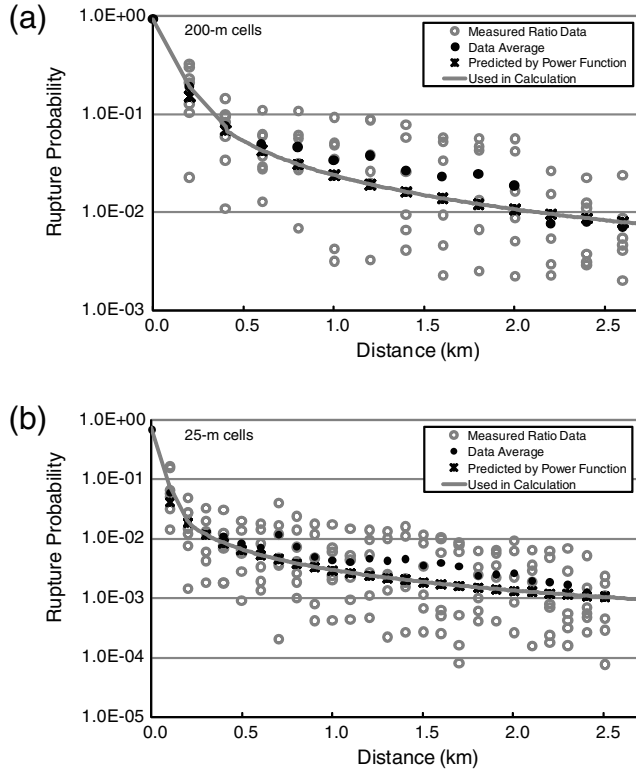


Figure 8. Probability of distributed-fault rupture displacement with regression equation and data averaged in bins for (a) 200 m \times 200 m cells and (b) 25 m \times 25 m cells.

$$(l/L)' = \frac{1}{b}[(a_2 - a_1)m + (c_2 - c_1)]. \quad (9)$$

Again, equation (7) is used when $l/L < (l/L)'$; otherwise, equation (8) is used. $(l/L)'$ is computed to range from 0.25 to 0.26 for earthquakes of all magnitudes considered in this study. Figure 5b shows the displacement data and regression analysis for an M 7.5 earthquake with the ± 1 and 2 standard deviations (sigmas).

We also performed a multivariate regression analysis on the parameters m , l/L , and $(l/L)^2$, which yielded the following quadratic equation of $\ln(D)$ with respect to l/L :

$$\ln(D) = 1.7895m + 14.4696(l/L) - 20.1723(l/L)^2 - 10.54512. \quad (10)$$

This regression has a standard deviation of 1.1346 in \ln units. According to this model, the maximum displacement does not occur at the middle point of the fault. Taking the partial derivative, $\partial[\ln(D)]/\partial(l/L)$, indicates that displacement peaks at l/l approximately equal 0.36. We assume that the peak is equally likely to occur near either end of the fault. The data and regression equations are shown in Figure 5c.

The elliptical model analysis assumes that the displacement data follows the upper left quarter of an ellipse centered at $l/L = 0.5$ and $\ln(D) = 0$. The equation of the ellipse in the l/L versus the $\ln(D)$ coordinate is

$$\frac{[(l/L) - 0.5]^2}{0.5^2} + \frac{[\ln(D)]^2}{b^2} = 1. \quad (11)$$

Rearranging equation (11) yields

$$\ln(D) = b\sqrt{1 - \frac{1}{0.5^2}[(l/L) - 0.5]^2} = bx^*. \quad (12)$$

We also performed a regression analysis for terms of x^* , a transformed form of l/L . Incorporating the earthquake magnitude term, we obtain the following regression equation:

$$\ln(D) = bx^* + am + c. \quad (13)$$

Here, we also added the intercept term as a regression coefficient. This eliminates the constraint made earlier with the assumption that one tip of the ellipse occurs at $[\ln(D) = 0, l/L = 0]$. Instead, the location of the top of the ellipse is determined through the regression process. Performing linear regression on equation (13) yielded $b = 3.3041$, $a = 1.7927$, and $c = -11.2192$, with a standard deviation on $\ln(D)$ of 1.1348. The data and regression equations are shown in Figure 5d. Biasi and Weldon (2006, 2009) used $[\sin(\pi l/L)]^{1/2}$ to approximate the distribution of displacement along the fault. Substituting x^* in equation (13) with this functional form yields $b = 3.1036$, $a = 1.7940$, $c = -11.0$, and a standard deviation on $\ln(D)$ of 1.1382. The regressions based on the Biasi and Weldon (2006, 2009) functional form compare well with our elliptical model (see Fig. 5d). In fact, the two models typically differ by less than 2% for 95% of the fault length but can differ by 5% up to 25% at the ends of the rupture.

Analysis of Normalized Principal-Fault Displacements

We developed the normalized principal-fault displacements by dividing the observed displacements by the average displacements calculated using the Wells and Coppersmith (1994) regression equation (equation 6) for a given magnitude. The advantage of using this normalized method for assessing fault displacements is that one can apply the Wells and Coppersmith (1994) global average displacement model for the magnitude of interest. The reason we chose the Wells and Coppersmith (1994) average-displacement model for this analysis is that we used this magnitude-displacement relation in our normalization of the displacement data and because this relation provides similar estimates to the geological mean displacements provided in the literature. Youngs *et al.* (2003) applied this same equation in their study. The three statistical models used in the principal-fault displacements were also used in the analysis of normalized principal-fault displacements: bilinear, quadratic, and elliptical models.

Fixing the D/D_{ave} value in the central portion of the fault at 1.0, we obtain the following bilinear model:

$$\ln(D/D_{\text{ave}}) = 8.2525(l/L) - 2.3010,$$

$$\sigma = 1.2962 \text{ in ln units for } l/L < (l/L)', \quad (14)$$

and

$$\ln(D/D_{\text{ave}}) = 0.1816,$$

$$\sigma = 1.0013 \text{ in ln units for } l/L \geq (l/L)', \quad (15)$$

where $(l/L)' = 0.3008$ is the l/L value at which the two linear portions intersect. Figure 5e shows the data normalized by the average displacement obtained from Wells and Coppersmith (1994) with the predicted uncertainties.

The quadratic model equation is given by

$$\ln(D/D_{\text{ave}}) = 14.2824(l/L) - 19.8833(l/L)^2 - 2.6279. \quad (16)$$

This regression yielded a standard deviation of 1.1419 in ln units.

Again, using a data transformation, we fit the distribution of $\ln(D/D_{\text{ave}})$ with respect to l/L into a portion of an elliptical shape (i.e., similar to equation 12, with the dependent variable being $\ln(D/D_{\text{ave}})$). Performing a linear regression on transformed data (x^*), we obtain the elliptical model equation

$$\ln(D/D_{\text{ave}}) = 3.2699x^* - 3.2749$$

$$\text{where } x^* = \sqrt{1 - \frac{1}{0.5^2}[(l/L) - 0.5]^2}. \quad (17)$$

The standard deviation in ln units for this regression is 1.1419.

Our analysis of the displacement data indicates that the bilinear model has the lowest aleatory variability for sites located near the middle of the fault and the highest at sites near the ends of the fault. Aleatory variability for the quadratic and elliptical equations are almost identical for principal-fault displacements. The uncertainties in the normalized equations are slightly lower than those for the magnitude- and distance-dependent equations. However, the former equations do not account for uncertainty in magnitude that is needed to calculate the average displacement.

Analysis of Distributed-Fault (Off-Fault) Displacements: Function of Magnitude and Distance

We performed regression analysis on the off-fault displacements and found a weak correlation with magnitude (m) and distance (r , in meters) from the rupture. Figure 7 shows the off-fault displacement data and regression lines for M 6.5 to 7.5 events.

Statistical analysis on distributed-fault displacement data shows that the relationship between d and r is best described by a power function: $d = ar^b$. The regression is performed on its transformed form (i.e., both d and r are

in ln terms by taking the natural log on both sides of the equation). Adding a linear dependence of m , we obtain

$$\ln(d) = 1.4016m - 0.1671 \ln(r) - 6.7991, \quad (18)$$

where d is in centimeters and r is in meters. This regression has a standard deviation of 1.1193 in ln units. The standard error for the slope of $\ln(r)$ is 0.0476. Based on the rule of thumb (i.e., if a coefficient estimate is more than 2 standard errors away from zero, then it is statistically significant; Gelman and Hill, 2007), the distance term is significant although the correlation is rather weak. Figure 7a shows the displacement data for distributed-fault ruptures along with the regression models for various earthquake magnitudes.

Analysis of Normalized Distributed-Fault (Off-Fault) Displacements

Again, using a power function, the off-fault displacement normalized by the average displacement for a given earthquake is found to be

$$\ln(d/D_{\text{ave}}) = -0.1826 \ln(r) - 1.5471, \quad (19)$$

where r is in meters. This regression has a standard deviation of 1.1388 in ln units, and standard error for the slope is 0.0483. Figure 7b shows the normalized off-fault displacements along with the regression curve and its uncertainties.

Probability of Ground Rupture for Distributed Faulting (Off-Fault)

We also analyzed the off-fault displacement data to calculate the probability for a rupture to occur (or conversely for a rupture to not occur) in a given cell area located off the principal fault. We analyzed the potential for distributed-fault displacement to pass through an area as a function of distance from the principal trace.

The area that a structure occupies is critical in calculating the probability of earthquake rupture at that site. Typically, smaller areas have lower probability of containing a rupture. We examined the probability of ground rupture in areas off of the principal fault of $25 \text{ m} \times 25 \text{ m}$, $50 \text{ m} \times 50 \text{ m}$, $75 \text{ m} \times 75 \text{ m}$, $100 \text{ m} \times 100 \text{ m}$, and $200 \text{ m} \times 200 \text{ m}$ (Fig. 8; Tables 4 and 5). The probability of surface displacements is high for sites very close to the fault. However, this frequency drops off quickly. The displacement data indicate that most displacements occur on or within a few hundred meters of the principal fault. Contrary to the results of Youngs *et al.* (2003), we found no magnitude dependence for this probability. For example at 1-km distance and for a $25 \times 25 \text{ m}^2$ cell, the Landers event has a 1 in 100 chance of having surface rupture while the Izmit earthquake has only a 1 in 1000 chance of having surface rupture. Several earthquakes smaller than Izmit have higher than 1 in 1000 chance of having surface rupture. We assume a power function,

$$\ln(P) = a(z) \ln(r) + b(z), \quad (20)$$

where $a(z)$ and $b(z)$ are regression coefficients and are functions of grid size, and r is fault distance. These parameters are listed in Tables 4 and 5 for the five grid sizes investigated in this study.

This power function, however, does not extrapolate well in areas within a few hundred meters of the fault. Therefore, for areas close to the fault (near field), rupture probability is linearly interpolated using the rupture probability (p_0) on the fault and the first two off-fault rupture probability measurements (p_1 at a distance of r_1 for the first point and p_2 at a distance of r_2 for the second point).

Example Applications

In this section, we present examples showing how fault-rupture hazard may be assessed for a fault with different accuracy and complexity characteristics along a transect oriented normal to the fault rupture or in a map view. To illustrate the methodology and data sets, we assume a fault that ruptures with a characteristic M 7 earthquake on average every 140 yr, resulting in a rate of 0.00714 earthquakes per year. We perform a probabilistic fault rupture hazard analysis using this single rupture source. We do not examine the effects of a Gutenberg–Richter magnitude-frequency distribution. For this example, we assume that the principal fault can occur within 2 standard deviations of the mapped fault trace with standard deviations given in Tables 2 and 3 and weights provided assuming a normal distribution. We consider the probability of fault rupture on the fault to be one and do not allow lack of surface rupture directly along the fault.

Figure 9 shows probabilistic displacement hazard profiles across a mapped fault trace to illustrate the sensitivity of these parameters. Figure 9a shows examples of calculated displacement hazards for a transect across a simple fault trace using 25×25 m cells and a bilinear regression model. We apply both the method 1 (magnitude-distance regression) and method 2 (normalized regressions with D_{ave}) approaches for three different exceedance probabilities, 10%, 5%, and 2% in 50 yr. The normalized regression model results in 20% larger displacements over the fault trace. This is expected because a normalized model includes additional uncertainty required to assess the on-fault average displacements using the magnitude-dependent Wells and Coppersmith (1994) relations. At distances beyond about 100 m, the curve shows very low displacements because the distributed, secondary ruptures have low probability of occurrence in $25 \text{ m} \times 25 \text{ m}$ cells, and the displacements off the fault are typically much lower than the on-fault displacements.

We show the differences between the three types of regression equations in Figure 9b. These curves, which are based on method-1 (magnitude-distance) regressions are very similar, especially the quadratic and elliptical models. The bilinear model gives displacements about 15% lower than the other models over the fault trace for these 10%

in 50-yr hazard values. The lower hazard for the bilinear model is caused by the lower standard deviation across the central portion of the rupture. Figure 9c shows the strong effect of different mapping accuracy categories on the hazard analysis. Our calculations indicate that accurately mapped traces have a standard deviation of about 27 m. However, the inferred traces have standard deviations almost three times as large. This higher uncertainty translates into increased hazard at distances beyond 100 m. We also consider the effect of simple traces with a single through-going fault trace and complex traces with complicated steps, jogs, bifurcations, or parallel fault strands. The complex fault traces that are inferred or concealed have large uncertainty, both having a standard deviation of about 116 m. This high uncertainty translates into significant displacements at distances out to a few hundred meters. Figure 9d shows that for the 10% probability of exceedance level, displacements greater than 20 cm occur out to about 150 m for concealed or inferred simple traces, while they occur out to nearly 300 m for inferred or concealed complex traces.

The rate and magnitude of the earthquake also impact the hazard analysis. Figure 9e shows examples in which we have varied these parameters. At a site directly over the fault, an M 7.5 earthquake that occurs on average every 140 yr gives a displacement that is about double that resulting from an M 7.5 earthquake that occurs every 280 yr or an M 7 event that occurs every 140 yr at a 10% probability of exceedance level. Figure 9f shows the same information as in the previous plots but for a 50-yr exceedance probability. The probability of exceeding 0.5-m displacements is about 18% while the probability of exceeding a 2-m displacement is much lower, about 5% in a 50 yr period.

Figure 10 shows hazard curves for fault-displacement hazard. Figure 10a depicts hazard curves for two sites located near an accurately mapped fault trace. The site closer to the fault trace (64 m) gives hazard rates that are significantly higher than a site located farther away from the mapped trace (120 m). This figure also depicts deaggregated hazard curves showing relative contributions of the on-fault and off-fault displacements to the total hazard. Figure 10b shows hazard curves at a distance of approximately 160 m for different mapping accuracies. The hazard is significantly higher for concealed or inferred mapped traces even if the site is located 160 m from the mapped trace.

Figure 11 shows an example hazard map for a fault trace through an urban area (this is only an example and should not be used directly in design). This map is produced for a 10% probability of exceedance in 50 yr using a $25 \text{ m} \times 25 \text{ m}$ cell size. In this case, an A-P zone is shown that defines the region where construction for habitation is limited. If lifelines or nonhabitable structures are located in this region, this map would define the displacements that have a 1 in 475 rate of exceedance or an annual exceedance rate of 0.0021. This type of map may be useful for planners or city officials who want advice on designing structures that account for the

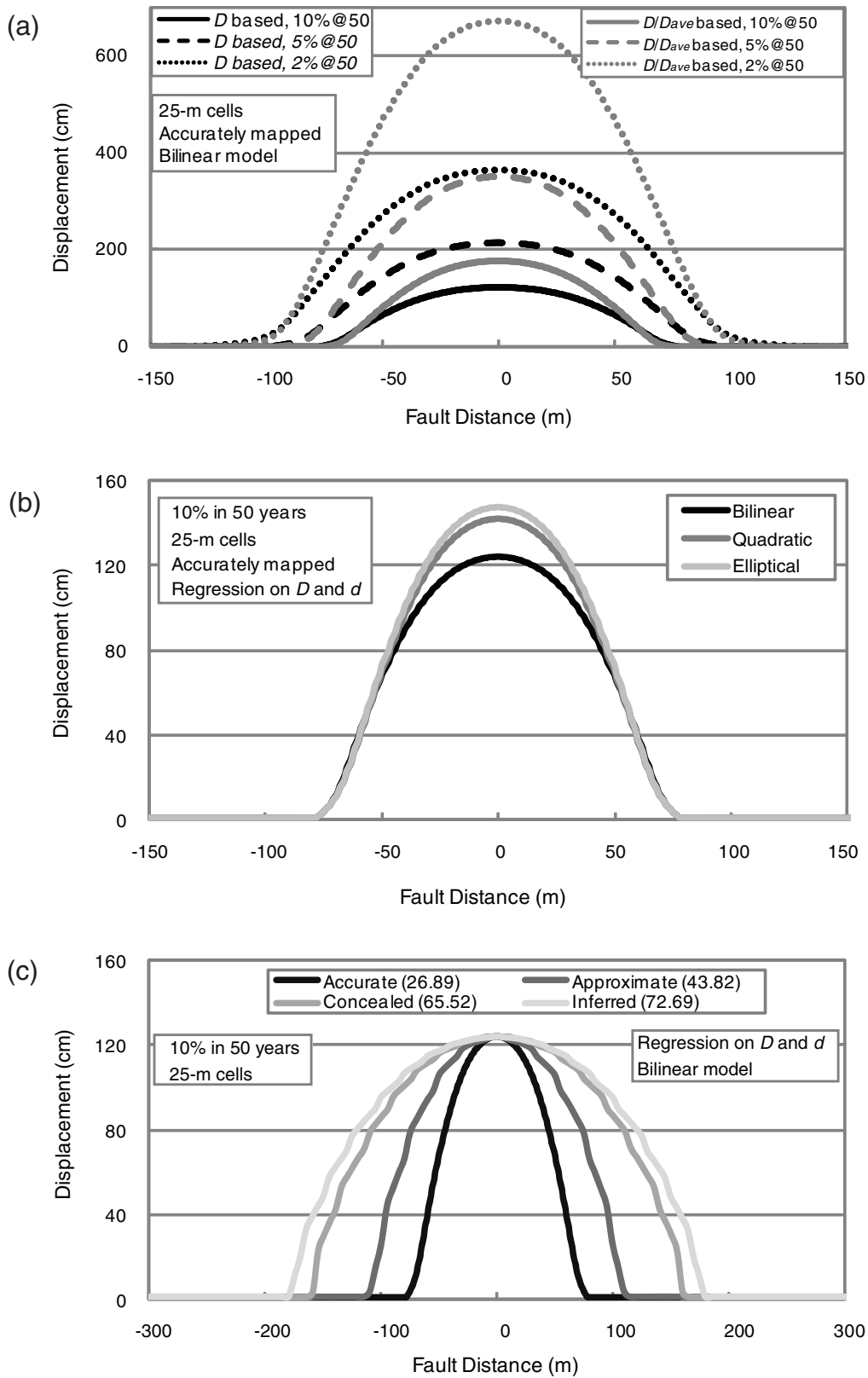


Figure 9. Calculated displacement hazard profiles: (a) Displacements across the fault—comparison of D -based and D/D_{ave} -based methods (10%@50 represents 10% exceedance probability in 50 yr, etc). (b) Displacements across the fault; comparison of different regression models. (c) Displacements across the fault; effect of mapping quality (standard deviations in meters are presented in parentheses). (d) Displacements across the fault; effect of fault complexity and mapping quality. (e) Displacements across the fault for different effects of earthquake magnitude and occurrence rates. (f) Probabilities of exceedance in 50 years for different displacement levels. (Continued)

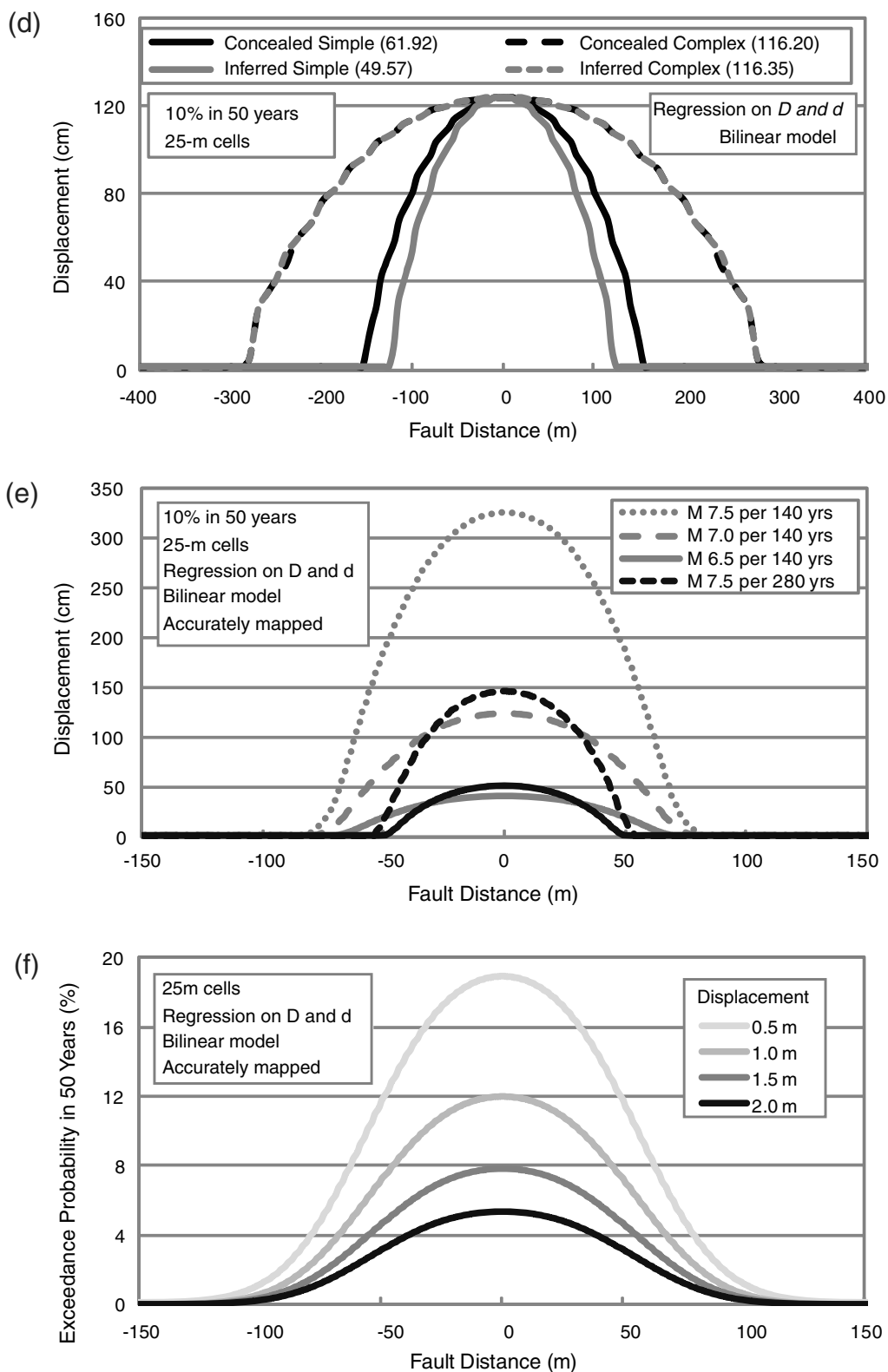


Figure 9. Continued.

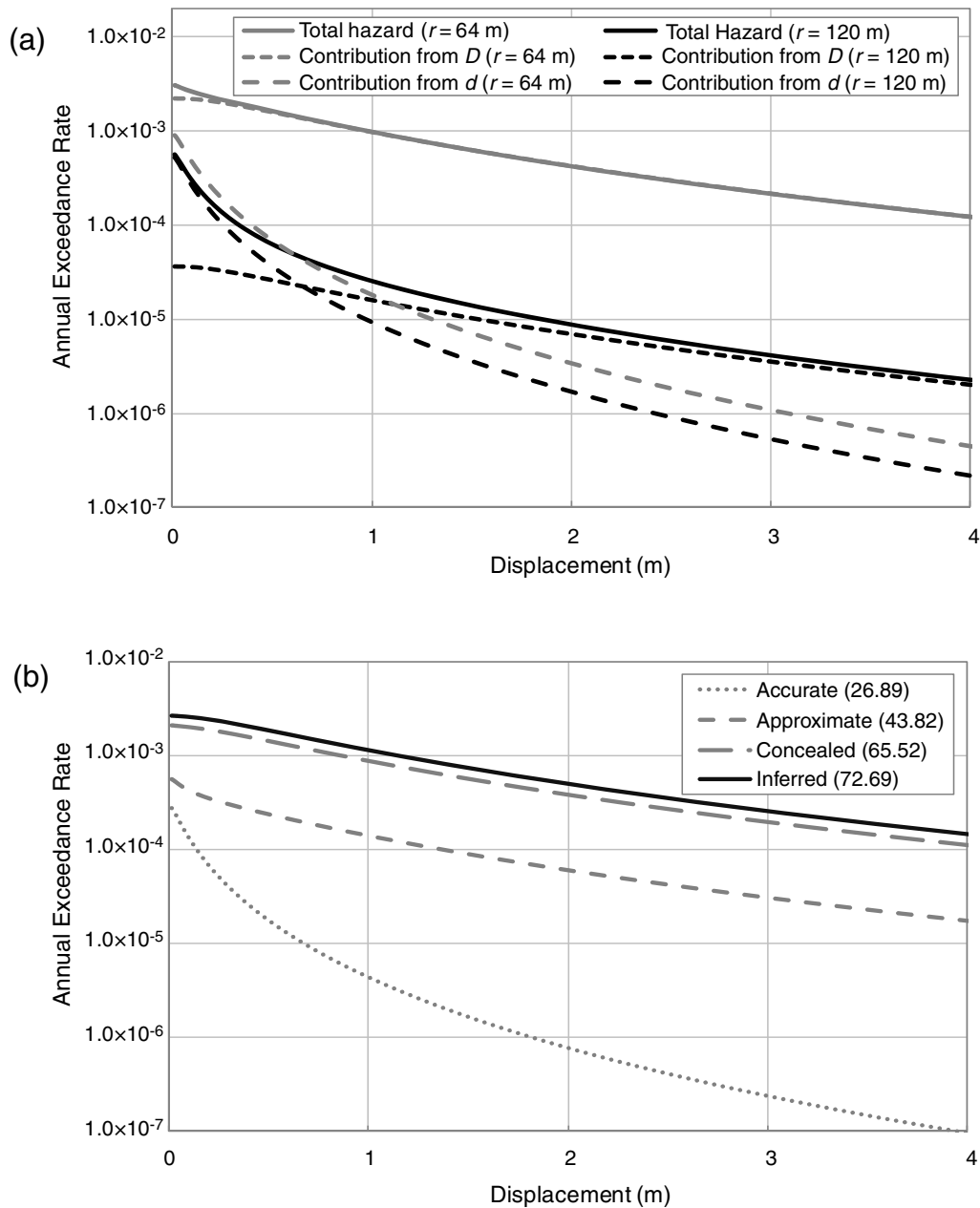


Figure 10. Comparison of displacement-hazard curves (a) along a profile perpendicular to the fault at two sites with fault distances of 64 m and 120 m for an accurately mapped fault and (b) at a distance of approximately 160 m for different mapping accuracies. In both figures, displacement-based regression, a bilinear model, and 25-m cells are assumed.

fault-rupture hazard and as a screening tool to identify sites prime for site-specific studies.

Discussion and Conclusions

We present a methodology for evaluating the hazard of fault displacement in a probabilistic and deterministic framework. In addition, we assembled a global database of surface-rupture displacements for large strike-slip earthquakes, applied these data to a GIS system for digital analysis, developed equations that define the distributions and parameters necessary for assessing the hazard, and compared

the fault rupture data with prerupture fault mapping to quantify the impact of mapping accuracy and complexity in predicting future displacements. Regressions for fault displacement indicate that magnitude, distance along the fault rupture, distance away from the rupture, fault mapping accuracy, and fault complexity are all important factors in predicting the locations and sizes of rupture displacements for strike-slip earthquakes. We applied three regression models to describe the displacements on the principal fault: bilinear, quadratic, and elliptical models. In addition, we regress the off-fault displacement data using a similar multivariate regression approach. The models for principal fault

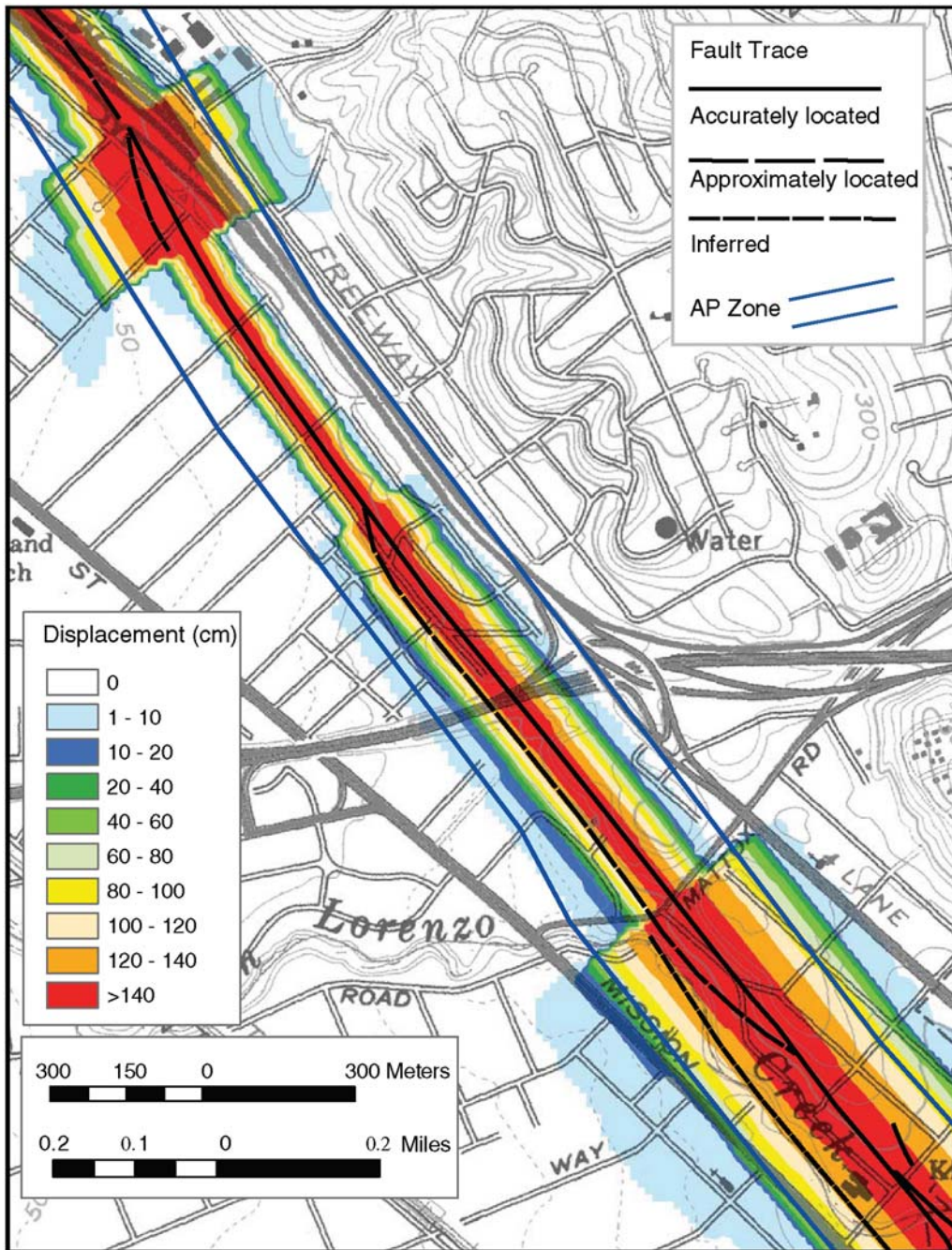


Figure 11. An example of a fault-displacement hazard map.

displacements differ in the level of aleatory uncertainty and in how the displacements decay at the end of the rupture. We prefer the multivariate regression models for magnitude and distance over the normalized models because they result in lower overall uncertainties. However, we do not have any basis for preferring one of the bilinear, quadratic, and elliptical models over another, because the calculated aleatory uncertainties are similar for each of the models. Assessment of the end points of the future ruptures may be difficult because the fault may be hidden or have variable rupture characteristics. One option for assessing fault-

displacement hazard would be to use a uniform displacement along the principal fault. If this analysis is desired, we would recommend using the middle portion of the bilinear regression model as the basis for these displacements.

For the off-fault displacement analysis, we recommend that the regression equations only be used out to 2 km because triggered displacements on other faults may be important out at larger distances. We have not accounted for these triggered displacements in this analysis. These data should be of use for engineers and earth scientists to evaluate the site-specific fault rupture hazard for a site near an active fault. These methods

may also be useful to screen areas for potential hazard where site-specific analyses may be needed or in places where bedrock faults are present and it is difficult to identify and date previous rupture displacements.

One of the most important results from this analysis indicates that, while observed ground displacements on the principal faults are generally quite large (often measured in meters), the displacements measured off the fault are generally only a few percent of the principal-fault displacements. Occasionally, however, these secondary ruptures were observed to exceed 1 m. Moreover, these centimeter-scale displacements may occur several kilometers from the primary fault, on distributed immature faults. If an engineering project is located near a fault but is insensitive to centimeter levels of displacement, then it is essential that an investigator ensures that the site is not located on the observed main strand or on unidentified faults located nearby. If the site is sensitive to centimeter-size displacements, then the engineer may need to design for fault rupture even if the site is located a few kilometers from the known earthquake source. This analysis does not take into account that earthquakes may also trigger events on other faults (e.g., 1992 Landers in the southern California rupture triggered the Big Bear earthquake on a different fault that was not considered in the seismic-hazard models). These neighboring faults should also be treated as separate principal faults.

Our model estimates the probability of a given magnitude of fault displacement considering a number of input parameters with both the model (epistemic) and random (aleatory) uncertainties in the assessment. The aleatory uncertainties for principal-fault and distributed-fault displacements are high, typically around a factor of 3 for one standard deviation. This is even higher than typical ground motion models which show scatter of about a factor of 2 for one standard deviation. Another important source of uncertainty is related to the locations of future ruptures. This uncertainty includes not only the aleatory variability associated with ruptures that do not repeat exactly, but also the epistemic uncertainty in producing a map. USGS map standards for 1:24,000 scale maps state that 95% of all objects on such a map will be within 40 ft of their actual location. It also includes the uncertainty in geologic interpretation. Even the most well-defined fault may be indicated by scarps or deflected drainages that are several meters wide. The geologic interpretation of a fault trace connecting such features will have an uncertainty of at least several meters. Additionally, even if a fault trace could be perfectly mapped, the rupture in a later earthquake may not precisely follow the previous trace. The uncertainty in fault rupture location, given a well-located fault mapped at a 1:24,000 scale, includes (1) the standard map error; any object on a 1:24,000 scale map has an uncertainty of 20 ft, which is an epistemic uncertainty in the location of the fault. (2) The geologic mapping error; any fault mapped based on surface expression of previous faulting will be accurate to within a few meters, which is an epistemic uncertainty in the location of the fault. (3) The random uncertainty in the location of fault

rupture from one earthquake to the next is considered an aleatory variability. Although we know the rough order of magnitude of each of these sources of error, we would need to determine these values more precisely to separate them in our analysis. For this reason, all three sources of error are all included in the location error between mapped faults and later fault ruptures. Because the standard deviation of the total location error is 18 m for well-located faults (Table 2), the epistemic uncertainties probably account for the majority of this error. If we knew the value of this aleatory uncertainty, we could use our model to calculate the probabilistic fault displacement for a site where the fault location is known from detailed surface and subsurface investigations. Future studies should focus on categorizing this aleatory variability and epistemic uncertainty so that we can more appropriately assess the PDFs applied in the displacement hazard analysis for strike-slip faults.

Data and Resources

The displacement data applied in this analysis were digitized from published sources shown in Table 1. These data were supplemented with displacement data published by Wesnousky (2008). We refer to published methodology and equations shown in references and web sites (e.g., <http://eqhazmaps.usgs.gov> and <http://conservation.ca.gov/cgs/>, last accessed January 2011). Almost all of the data and analysis results are provided in the  electronic supplement to this paper. Any use or trade, product, or firm names is for descriptive purposes only and does not imply endorsement by the U.S. Government. For a description of the 1972 Alquist-Priolo Earthquake Fault Zoning Act and implementation, see <http://www.conservation.ca.gov/cgs/rghm/ap/> (last accessed January 2011). U.S. fault data can be accessed at the websites: <http://eqhazmaps.usgs.gov>, <http://wgcep.org>, and <http://www.conservation.ca.gov/cgs> (last accessed January 2011).

Acknowledgments

We thank the Pacific Earthquake Engineering Research Center (PEER Lifelines project# 1J02, 1J02, and 1J03) advisory groups that assisted us in the formulation and implementation of these results. The members were Norm Abrahamson and Lloyd Cluff of Pacific Gas and Electric, Brian Chiou and Cliff Roblee from the California Department of Transportation, Bill Bryant from the CGS, Jon Bray from the University of California, Berkeley, Tom Rockwell from San Diego State University, Donald Wells and Bob Youngs from AMEC-Geomatrix, and Clarence Allen from the California Institute of Technology. We also thank the PEER Lifelines and USGS Earthquake Program which funded the studies. Nicolas Luco, Charles Mueller, Stephen Harmsen, Patricia Thomas, Stephen Thompson, Ivan Wong, and Melanie Walling reviewed the manuscript and provided helpful suggestions for improving the paper.

References

- Akyuz, H. S., R. Hartleb, A. Barka, E. Altunel, G. Sunal, B. Meyer, and R. Armijo (2002). Surface rupture and slip distribution of the 12

- November 1999 Duzce earthquake (M 7.1), North Anatolian fault, Bolu, Turkey, *Bull. Seismol. Soc. Am.* **92**, 61–66.
- Awata, Y., and K. Mizuno (1998). Strip map of the surface fault ruptures associated with the 1995 Hyōgo-Ken Nanbu earthquake, Central Japan—The Nojima, Ogura, and Nadagawa earthquake faults, *Geol. Surv. of Japan Tectonic Map Series 12*, scale 1:10,000.
- Ben-Zion, Y., and C. Sammis (2003). Characterization of fault zones, *Pure Appl. Geophys.* **160**, 677–715.
- Biasi, G. P., and R. J. Weldon (2006). Estimating surface rupture length and magnitude of paleoearthquakes from point measurements of rupture displacement, *Bull. Seismol. Soc. Am.* **96**, 1612–1623.
- Biasi, G.P., and R. Weldon (2009). San Andreas fault rupture scenarios from multiple paleoseismic records: Stringing pearls, *Bull. Seismol. Soc. Am.* **99**, 471–498.
- Braun, J. B. (2000). Probabilistic fault displacement hazards of the Wasatch fault, *Master's Thesis*, Department of Geology and Geophysics, The University of Utah, Salt Lake City, Utah.
- Clark, M. M. (1972). Surface rupture along the Coyote Creek fault, the Borrego Mountain Earthquake of April 9, 1968, *U.S. Geol. Surv. Profess. Pap.* **787**, 55–57.
- Fialko, Y., M. Simons, and D. Agnew (2001). The complete (3-D) surface displacement field in the epicentral area of the 1999 M_w 7.1 Hector Mine earthquake, California, from space geodetic observations, *Geophys. Res. Lett.* **28**, 3063–3066.
- Frankel, A. D., M. D. Petersen, C. S. Mueller, K. M. Haller, R. L. Wheeler, E. V. Leyendecker, R. L. Wesson, S. C. Harmsen, C. H. Cramer, and D. M. Perkins (2002). Documentation for the 2002 update of the national seismic hazard maps, *U.S. Geol. Surv. Open-file Rept. 02-420*.
- Gelman, A., and J. Hill (2007). *Data Analysis Using Regression and Multilevel/Hierarchical Models*, Cambridge University Press, New York.
- Hemphill-Haley, M. A., and R. J. Weldon II (1999). Estimating prehistoric earthquake magnitude from point measurements of surface rupture, *Bull. Seismol. Soc. Am.* **89**, 1264–1279.
- Langridge, R., H. D. Stenner, T. E. Fumal, S. A. Christofferson, T. K. Rockwell, R. D. Hartleb, J. Bachhuber, and A. A. Barka (2002). Geometry, slip distribution, and kinematics of surface rupture on the Sakarya segment during the 17 August Izmit, Turkey earthquake, *Bull. Seismol. Soc. Am.* **92**, 107–125.
- Petersen, M. D., and S. G. Wesnousky (1994). Fault slip rates and earthquake histories for active faults in southern California, *Bull. Seismol. Soc. Am.* **84**, 1608–1649.
- Petersen, M. D., W. A. Bryant, C. H. Cramer, T. Cao, M. S. Reichle, A. D. Frankel, J. J. Lienkaemper, P. A. McCrory, and D. P. Schwartz (1996). Probabilistic seismic hazard assessment for the state of California, *California Division of Mines and Geol. Open-file Rept. 96-08 and U.S. Geol. Surv. Open-file Rept. 96-706*.
- Petersen, M. D., A. D. Frankel, S. C. Harmsen, C. S. Mueller, K. M. Haller, R. L. Wheeler, R. L. Wesson, Y. Zeng, O. S. Boyd, D. M. Perkins, N. Luco, E. H. Field, C. J. Wills, and K. S. Rukstales (2008). Documentation for the 2008 update of the United States national seismic hazard maps, *USGS Open-File Rept. 2008-1128*, 60 pp. (11 appendices).
- Sharp, R. V., J. J. Lienkaemper, M. G. Bonilla, D. B. Burke, B. F. Fox, D. G. Herd, D. M. Miller, D. M. Morton, D. J. Ponti, M. J. Rymer, J. C. Tinsley, J. C. Yount, J. E. Kahle, E. W. Hart, and K. E. Sieh (1982). Surface faulting in the Central Imperial Valley in the Imperial Valley, California, earthquake of October 15, 1979, *U.S. Geol. Surv. Prof. Pap.* **1254**, 119–154 and Plate 1.
- Sharp, R., K. Budding, J. Boatwright, M. Ader, M. Bonilla, M. Clark, T. Fumal, T. Harms, J. Lienkaemper, D. Morton, B. O'Neill, C. Ostergren, D. Ponti, M. Rymer, J. Saxton, and J. Sims (1989). Surface faulting along the Superstition Hills fault zone and nearby faults associated with the earthquakes of 24 November 1987, *Bull. Seismol. Soc. Am.* **79**, 252–281.
- Sorensen, S. P., and K. J. Meyer (2003). Effect of the Denali fault rupture on the Trans-Alaska pipeline, *Proc. Sixth U.S. Conf. and Workshop on Lifeline Earthq. Eng.*, ASCE Technical Council on Lifeline Earthquake Engineering, August 2003, 9 pp.
- Stepp, J. C., I. Wong, J. Whitney, R. Quittmeyer, N. Abrahamson, G. Toro, R. Youngs, K. Coppersmith, J. Savy, T. Sullivan, and Yucca Mountain PSHA Project Members (2001). Probabilistic seismic hazard analyses for ground motions and fault displacement at Yucca Mountain, Nevada, *Earthq. Spectra* **17**, 113–150.
- Treiman, J. A., K. J. Kendrick, W. A. Bryant, T. K. Rockwell, and S. F. McGill (2002). Primary surface rupture associated with the M_w 7.1 16 October 1999 Hector Mine earthquake, San Bernardino County, California, *Bull. Seismol. Soc. Am.* **92**, 1171–1191.
- Wells, D. L., and K. J. Coppersmith (1993). Likelihood of surface rupture as a function of magnitude, *Seismol. Res. Lett.* **64**, 54 (abstract).
- Wells, D. L., and K. J. Coppersmith (1994). New empirical relationships among magnitude, rupture length, rupture width, rupture area, and surface displacement, *Bull. Seismol. Soc. Am.* **84**, 974–1002.
- Wesnousky, S. G. (2008). Displacement and geometrical characteristics of earthquake surface ruptures, *Bull. Seismol. Soc. Am.* **98**, 1609–1632.
- Youngs, R. R., W. J. Arabasz, R. E. Anderson, A. R. Ramelli, J. P. Ake, D. B. Slemmons, J. P. McCalpin, D. I. Doser, C. J. Fridrich, F. H. Swan III, A. M. Rogers, J. C. Yount, L. W. Anderson, K. D. Smith, R. L. Bruhn, L. K. Knuepfer, R. B. Smith, C. M. dePolo, K. W. O'Leary, K. J. Coppersmith, S. K. Pezzopane, D. P. Schwartz, J. W. Whitney, S. S. Olig, and G. R. Toro (2003). A methodology for probabilistic fault displacement hazard analysis (PFDHA), *Earthq. Spectra* **19**, 191–219.

U.S. Geological Survey
1711 Illinois Street
Golden, Colorado 80401
mpetersen@usgs.gov
(M.D.P.)

California Geological Survey
345 Middlefield Road, MS 520
Menlo Park, California 94025
(T.E.D.)

California Geological Survey
801 K Street, MS 12-32
Sacramento, California 95814
(R.C., C.J.W.)

U.S. Nuclear Regulatory Commission
11555 Rockville Pike, MS B2 E2
Washington, D.C. 20555-0001
(T.C.)

U.S. Geological Survey
345 Middlefield Road, MS 977
Menlo Park, California 94025
(D.P.S.)

U.S. Geological Survey
University of Washington
Dept of Earth and Space Science
Seattle, Washington 98915
(A.D.F.)